IOPscience iopscience.iop.org

Home Search Collections Journals About Contact us My IOPscience

The effect of varying substrate temperature on the structural and optical properties of sputtered GaAs films

This article has been downloaded from IOPscience. Please scroll down to see the full text article.

1993 J. Phys.: Condens. Matter 5 519

(http://iopscience.iop.org/0953-8984/5/5/003)

View the table of contents for this issue, or go to the journal homepage for more

Download details:
IP Address: 171.66.16.96
The article was downloaded on 11/05/2010 at 01:04

Please note that terms and conditions apply.

J. Phys.: Condens. Matter 5 (1993) 519–534. Printed in the UK

The effect of varying substrate temperature on the structural and optical properties of sputtered GaAs films

S H Baker†, S C Bayliss‡, S J Gurman†, N Elgun†, J S Bates‡ and E A Davis†

† *Department of Physics and Astronomy, University of Leicester, Leicester LE1 7RH, UK*

‡ Department of Physics, Loughborough University of Technology, Loughborough, Leicestershire LE11 3TU, UK

Received 4 September 1992, in final form 6 November 1992

Abstract. Stoichiometric GaAs films have been prepared by RF sputtering over an appreciable range of substrate temperature T_s. The structural and optical properties of these films have been investigated by means of a variety of experimental techniques. Transmission electron microscope (TEM) experiments reveal that for $T_s \geqslant \sim 70$ °C the structure consists of nanocrystals embedded in an amorphous network. EXAFS, XPS and infrared experiments are consistent with each other, indicating that configurational disorder in the amorphous network of the GaAs films decreases as T_s is raised. Most of the disorder relates to bond-angle disorder; the spread in bond angle around Ga atoms is found to be less than that around As atoms for a given substrate temperature. The changes observed in the fundamental absorption edge with increasing T_s are discussed in relation to various possible defects in amorphous GaAs.

1. Introduction

Previous work on amorphous III–V semiconductors has focused mostly on stoichiometric (or near-stoichiometric) compounds. Early x-ray diffraction studies on such compounds [1] showed, as in the case of a-Si and a-Ge, that although they lacked the long-range order of the corresponding crystal structure they retained tetrahedral short-range order. The first continuous random network (CRN) model proposed for the structure of a-Si and a-Ge (by Polk [2]) contains a considerable number of odd-membered rings; in the case of amorphous III–V compounds, this would necessarily introduce a proportion of wrong bonds, i.e. bonds between like atoms. A CRN model introduced by Connell and Temkin [3], consisting only of even-membered rings, was suggested to be possibly more appropriate. Electron diffraction studies on near-stoichiometric a-GaAs, a-GaP, a-GaSb and a-InP by Dixmier *et al* [4] supported this view.

The adoption of the Connell–Temkin CRN implies a high degree of chemical order. Further information on the extent of chemical ordering in amorphous III–V materials has been obtained from a variety of experiments. On the basis of EXAFS [5] and optical [6] measurements, Theye and co-workers concluded that flash-evaporated (stoichiometric) a-GaAs contained few wrong bonds. This is in general agreement with an EXAFS and optical study by Baker *et al* [7] on sputtered a-$Ga_{1-x}As_x$ (0.5

0953-8984/93/050519+16$07.50 © 1993 IOP Publishing Ltd

$\leqslant x \leqslant 0.85$), although the inability to distinguish between Ga and As scatterers somewhat hampered EXAFS analysis; the extension to As-rich specimens allowed the authors to detect a change in coordination around As atoms from about four at compositions close to stoichiometry towards about three in very As-rich films (Ga atoms remained fourfold coordinated over the composition range investigated). In the case of a-GaP, however, contrary results have been obtained by different groups. EXAFS studies [5, 8] on approximately stoichiometric flash-evaporated a-GaP provide evidence for both Ga–Ga and P–P bonds, with the proportion of wrong bonds apparently as high as 25%. The electron diffraction experiments of Dixmier *et al* [4] suggest that this partial chemical disorder is not forced on the network by topological considerations; instead, the authors attribute it to 'extrinsic' disorder arising from the particular method of sample preparation. Indeed, recent EXAFS and optical experiments on sputtered (approximately stoichiometric) a-GaP [9] indicate a much higher degree of chemical ordering, with no wrong bonds detectable (at least within the sensitivity of the EXAFS and infrared experiments carried out in this study).

The preparation conditions, in particular the substrate temperature, necessary for the deposition of amorphous (as opposed to microcrystalline) III–V materials differ quite widely among the various reports in the literature. In the case of GaAs, Paul *et al* [10] found that films sputtered from an Ar/H_2 plasma were partially crystalline when the substrate temperature was around or above 25 °C; a temperature of 4 °C was required to produce fully amorphous material. However, Hargreaves *et al* [11] were able to prepare a-GaAs by sputtering at up to 30 °C. Furthermore, MBE-deposited GaAs can apparently be prepared in amorphous form at substrate temperatures as high as 200 °C or more [12]. In view of the differences in preparation conditions mentioned above, it appeared to us to be of interest to prepare a set of sputtered GaAs films over an appreciable range of substrate temperatures T_s in an attempt to determine the point at which the deposited films first show signs of microcrystallinity (at least for our deposition system). There appear to have been few systematic investigations into the effect on the structural and electronic properties of amorphous III–V semiconductors of varying preparation conditions such as T_s, which would be expected to produce changes in the configurational disorder of the amorphous network (i.e. variations in bond angle and bond length). The second principal aim of our work was therefore to study the effect of reducing the degree of configurational disorder in amorphous GaAs films, through increases in T_s. In what follows, we present and discuss the results of TEM, EXAFS, optical (including infrared) and XPS measurements on a set of GaAs films prepared over a wide range of substrate temperature.

2. Preparation

The GaAs films were prepared by RF sputtering in an argon atmosphere at a pressure of ~4 mTorr. The base pressure of the system was 2×10^{-7} Torr or better. An RF power of 75 W was applied to the target which was a crystalline GaAs wafer, 2 inches in diameter. The sputtered films were deposited onto a variety of substrates: Corning 7059 for optical measurements, c-Si for infrared work, mylar for EXAFS experiments and Al foil for composition and XPS measurements. Substrate temperatures T_s above and below room temperature were achieved by means of a substrate table heater and temperature controller and by water-cooling respectively. The T_s range investigated

was 14 °C–240 °C. The thicknesses of the deposited films lay between 0.09 and 0.16 μm.

3. Microstructure

The composition of the GaAs films was determined by energy dispersive x-ray analysis (EDAX) using a DS130 scanning electron microscope (SEM). All samples were found to be essentially stoichiometric, with deviations from stoichiometry of no more than 3 or 4 at.%. No significant variations in composition were found between different areas of the same sample, suggesting that the GaAs films were compositionally homogeneous, at least down to a scale of 5 μm × 5 μm (the area probed by the EDAX measurements).

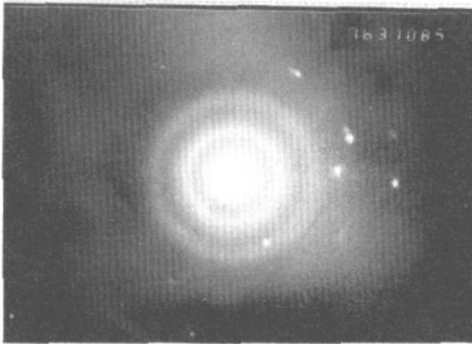

Figure 1. Electron diffraction pattern for GaAs sample prepared at 53 °C.

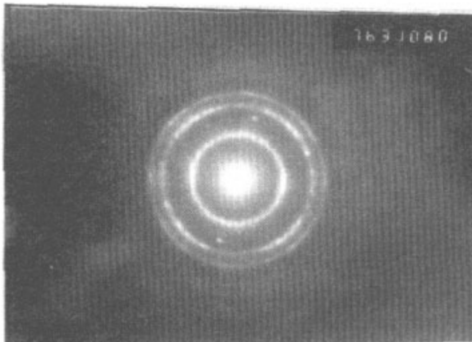

Figure 2. Electron diffraction pattern for GaAs sample prepared at 72 °C.

The microstructure of the sputtered GaAs samples was also investigated by means of transmission electron microscopy (TEM) experiments, carried out using a Jeol JEM 100 CX instrument. For each sample, the composition was checked *in situ* by EDAX prior to carrying out TEM measurements. In the case of films prepared at substrate

temperatures of ~50 °C or less, the diffraction patterns consist of a few diffuse rings, as in figure 1, confirming the amorphicity of these samples; micrographs recorded in real space, as opposed to reciprocal space, show no evidence for any nanocrystals of diameter greater than 20 Å, the resolution of the microscope. At a slightly higher substrate temperature T_s of ~70 °C, the rings in the electron diffraction pattern become much thinner with brighter regions (see figure 2), while the micrograph reveals the presence of regularly distributed and similarly sized inhomogeneities (presumed to be nanocrystallites) of ~20 Å in diameter. As T_s is further raised, the rings fade and bright spots appear in the diffraction patterns, as in figure 3, which indicate an increasing degree of microcrystallinity. The micrographs reveal that the size of the nanocrystallites increases with rising T_s, although from 120 °C onwards they become more irregularly distributed and show a greater variation in size. The average nanocrystallite diameter reaches 100 Å at $T_s \simeq$ 180 °C. Without a clear idea of the thickness of the TEM samples, it is difficult to estimate the volume fraction occupied by the nanocrystals; nevertheless, the micrographs indicate that even for the samples deposited at highest T_s, amorphous material accounts for a substantial fraction. The diffraction pattern obtained from the sample prepared at 180 °C yielded lattice spacings which correlated well (to within ±0.1 Å) with values obtained for a c-GaAs wafer.

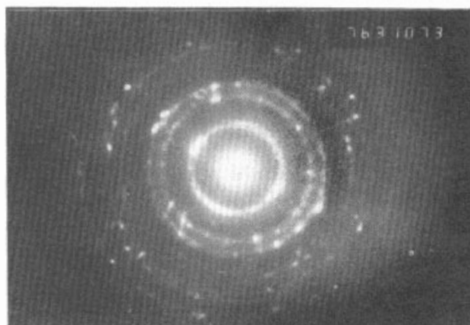

Figure 3. Electron diffraction pattern for GaAs sample prepared at 122 °C.

4. Experimental details

4.1. EXAFS

EXAFS measurements on the GaAs samples were carried out using the 2 GeV synchrotron radiation source at Daresbury Laboratory. The x-ray absorption coefficient μ was measured about both Ga and As K edges on station 7.1, which has a Si(111) double crystal monochromator. Measurements were made using standard transmission geometry, the beam intensities being measured by ionization chambers containing an Ar/He gas mixture. Harmonic rejection was set at 70% by detuning the monochromator. Samples were deposited onto low-absorbing mylar substrates for EXAFS studies; in order to obtain the necessary sample thickness, several layers were stacked together.

The EXAFS spectra were extracted from the measured absorption spectra $\mu(E)$ using the standard Daresbury program EXBACK [13]. This fits low-order polynomials to the pre- and post-edge data to represent the smoothly varying background absorption; these are then subtracted from the measured spectra to yield the EXAFS spectra $\chi(E)$.

A simplified expression, based on plane-wave theory, for the EXAFS function for K edges is given by

$$\chi(k) = -[A(k)/k] \sum_j \left(N_j/r_j^2\right) |f_j(\pi)| \exp\left(-2\sigma_j^2 k^2\right) \exp(-2r_j/\lambda) \sin(2kr_j + 2\delta + \psi) \tag{1}$$

where k, the photoelectron wavevector, is related to photon energy by

$$(\hbar^2 k^2)/2m = (\hbar\omega - E_{edge}) + E_0. \tag{2}$$

The energy of the edge E_{edge} is taken to be the point at which the first derivative of the absorption is a maximum. E_0, an energy offset, is the difference in energy between a $k = 0$ photoelectron and the lowest unoccupied energy level. N_j is the number of atoms of type j at a distance r_j from the absorbing atom, each of which has a back-scattering amplitude $|f_j(\pi)|$ (a function of both atom type and photoelectron energy). The factor $A(k)$ corrects for amplitude reductions due to events that result in absorption but not EXAFS, such as multiple electron excitations. In practice, $A(k)$ is taken to be independent of energy. The first exponential term in equation (1) is the Debye–Waller factor, describing the effects of vibrational and static disorder; σ_j^2 is the mean square variation in bond length r_j. The second exponential factor in the expression for χ represents losses due to inelastic scattering, λ being the elastic mean free path of the photoelectron. This is modelled in terms of a constant imaginary part of the potential V_i so that $\lambda = k/V_i$. This reproduces the $E^{1/2}$ variation of electron mean free path. δ is the phaseshift experienced by the photoelectron during its passage through the central atom potential, while ψ is the phase of the back-scattering factor.

Values for structural parameters such as r_j, N_j, etc can be obtained from the experimental EXAFS by fitting the experimental data to calculated EXAFS functions. In the case of our GaAs samples, structural information was obtained by multi-parameter fitting the experimental EXAFS spectra to EXAFS functions calculated using the fast curved-wave theory of Gurman *et al* [14]. The curve-fitting procedure was carried out with the aid of the EXCURV90 program [13] (readily available at Daresbury), which uses a least-squares analysis. Scattering phaseshifts were calculated within the program. $A(k)$ and V_i were obtained from an EXAFS study on a crystalline GaAs sample, which was also used to check the phaseshifts. The analysis program also contains a statistical package which gives the uncertainties on the structural parameters (often strongly correlated). We always quote the limits of the 95% confidence region, i.e. the $\pm 2\sigma$ uncertainties, where σ is the standard deviation.

4.2. XPS

X-ray photoelectron spectroscopy (XPS) data were taken from the as-grown GaAs films on aluminium substrates and from a crystalline GaAs wafer, using Al Kα

radiation at 1486.6 eV in a VG Escalab spectrometer. Scans were made over a binding energy range of 0–1200 eV and were calibrated using the oxygen 1s line at 532 eV and the oxygen Auger line at 976 eV. The absolute energy resolution (FWHM or full-width-at-half-maximum) of the instrument was 1.0 eV. The samples were not sputter-cleaned as this causes structural rearrangement. Since the films were not grown *in situ*, surface oxidation is evident in the core level spectra. At this resolution, however, it is possible to separate out the oxygenated components of the levels since the oxides produce chemical shifts of the order of 1 eV and 4 eV for Ga and As respectively.

4.3. Optical absorption measurements

Infrared transmission spectra for the GaAs films were recorded on a Perkin–Elmer 580B double-beam spectrophotometer over the wavenumber range 4000–180 cm^{-1}. The sample chamber was thoroughly purged with dry air during data-taking in order to reduce absorption due to water vapour.

Measurements at visible and near-infrared photon energies were carried out using a Perkin–Elmer 330 double-beam spectrophotometer, the absorption coefficient α being obtained by standard transmission and reflection techniques. α was also measured by PDS (photothermal deflection spectroscopy) in order to extend the range of measurable absorption coefficients to lower values than could be obtained by the transmission and reflection measurements.

5. Results

5.1. EXAFS

Examples of As-edge EXAFS spectra χ (weighted by k^3) for the sputtered GaAs films, together with the associated Fourier transforms, are given in figure 4. Data for a crystalline GaAs sample are also included. The noise level was sufficiently low to give a useable k range out to beyond 13 $Å^{-1}$, except for the crystalline sample where a larger data range was possible. The Fourier transforms are phase-corrected (taken with respect to $2kr + 2\delta + \psi$) so that the peaks appear at the true interatomic distances. For the sample prepared at 14 °C, the virtual absence of a second peak in the Fourier transform indicates considerable configurational disorder in the structural network. At higher substrate temperatures, a second peak (albeit a rather small one) is observed which suggests a reduction in the amount of disorder; this will be discussed in more detail later. The second peak in the Fourier transforms of the sputtered samples was always found to be much smaller than for the crystalline case, even at the highest substrate temperatures studied.

A problem associated with the data analysis (outlined in section 4.1) is that Ga and As atoms have very similar back-scattering amplitudes and phaseshifts, since they are very close to one another in atomic number. This means that they are virtually indistinguishable as scatterers. We have therefore assumed that around each Ga or As absorbing atom there is one basic atom type X, where X denotes either a Ga or an As atom. Changing X from As to Ga (or vice versa) hardly affected the fitted structural parameters, altering them by much less than their uncertainties. However, in spite of the difficulty referred to above, the data in a structural study by us on a-$Ga_{1-x}As_x$ [7] were not inconsistent with there being relatively few wrong bonds (like-atom bonds)

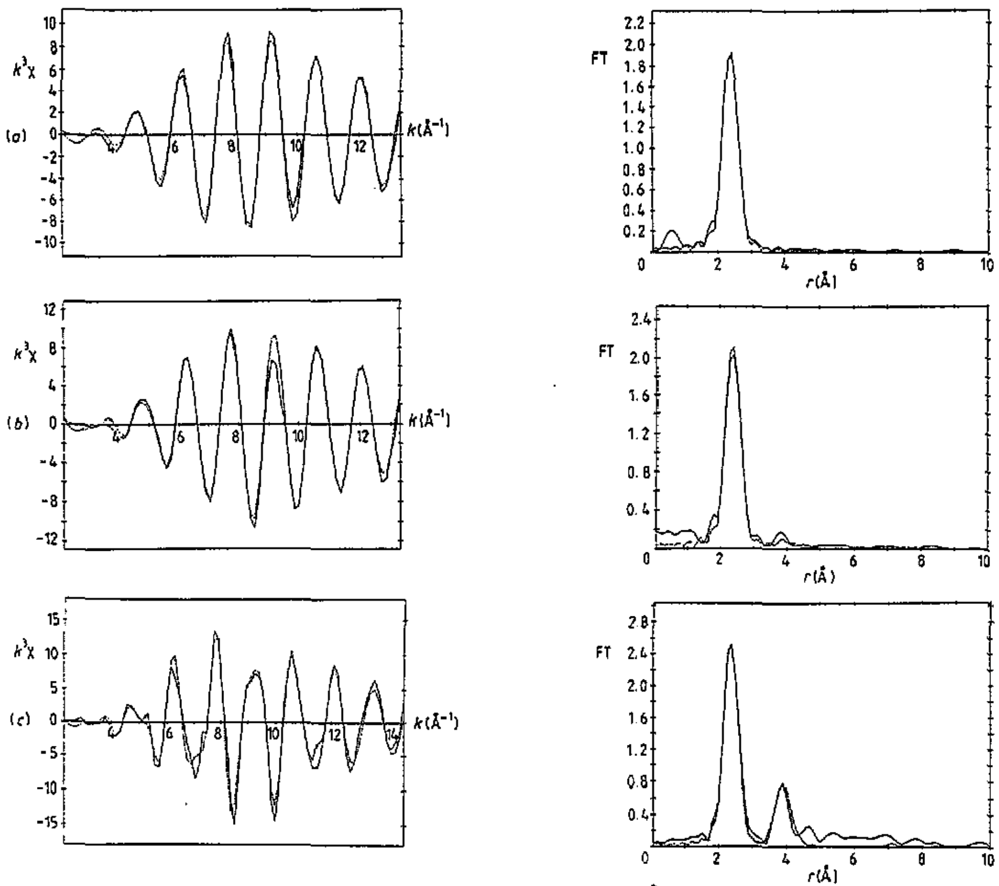

Figure 4. As-edge EXAFS spectra χ (weighted by k^3) and associated Fourier transforms (FT) for (*a*) GaAs sample prepared at 14 °C, (*b*) GaAs sample prepared at 122 °C and (*c*) crystalline GaAs sample. The full curves represent the experimental data; the broken curves give the best fit.

at stoichiometry. In fact, by calculating Penn gaps from measured refractive indices and plasmon energies, it has recently been demonstrated that a-GaAs (and a-InP) appear to be chemically ordered [15]. (This technique has been successfully applied to the amorphous alloys SiN_x [16] and SiO_x [17], both of which were found to be chemically ordered.) Furthermore, our XPS data (presented in section 5.2) strongly suggest that the sputtered GaAs samples are well chemically ordered.

Analysis of EXAFS data from the GaAs crystal yielded nearest-neighbour distances of 2.43 ± 0.02 Å (from Ga-edge data) and 2.42 ± 0.02 Å (from As-edge data), with a coordination N and Debye–Waller factor (from both edges) of 4.0 ± 0.5 and 0.005 ± 0.001 Å^2 respectively when the amplitude parameter $A(k)$ was set at 0.7 and the mean free path parameter V_i at −3 eV. Both sets of data are consistent, although the deduced bond length is slightly short; the bond length in c-GaAs is 2.45 Å. This points towards a slight error in our phaseshifts but does not, however, affect the conclusions in this study.

Fitting the first peak in the Fourier transforms for the sputtered GaAs samples proved fairly straightforward. With values of $A(k)$ and V_i identical to those used

for the crystal, both Ga- and As-edge data yielded bond lengths r_1 of 2.42 or 2.43 Å (±0.02 Å), a coordination N_1 of 4±1 and a Debye–Waller factor σ_1^2 of 0.006 ± 0.001 Å^2 in all cases. No significant variation with substrate temperature was found for any of the above parameters. This is in very good agreement with previous work [7] where it was also found that the fitted (first-shell) structural parameters for stoichiometric a-GaAs were nearly identical to those for c-GaAs. In particular, the close similarity in Debye–Waller factors between the two phases indicates that the major contribution to σ^2 in the amorphous samples is thermal or vibrational and that there is little static disorder in the bond length. Most of the configurational disorder in our GaAs samples is therefore associated with bond-angle disorder.

As we have already seen in figure 4, a second peak appears in the Fourier transforms of the EXAFS spectra as the substrate temperature T_s is increased. Clearly, fitting such small features with a reasonable degree of certainty is difficult. In an attempt to provide some quantitative analysis, we allowed the second-shell distance r_2 and Debye–Waller factor σ_2^2 to vary in the fitting procedure but kept the second-shell coordination N_2 fixed at 12 (as in c-GaAs). Analysis of As-edge EXAFS spectra for the GaAs films yielded σ_2^2 values which decreased as T_s was raised. This is illustrated in figure 5, which shows σ_2^2 as a function of T_s. (EXAFS measurements could not be carried out for samples deposited above 200 °C since the mylar substrates became unstable at these temperatures.) Values for r_2 (corresponding to the As–As distance assuming chemical ordering) lay between 3.95 and 3.99 Å. The uncertainties in σ_2^2 and r_2 are ±0.010 Å^2 and ±0.06 Å respectively. As-edge data from the crystalline GaAs sample gave second-shell parameters r_2 and σ_2^2 of 3.95 ± 0.03 Å and 0.012 ± 0.004 Å^2 respectively. The second-shell peaks in the Fourier transforms of Ga-edge spectra were much smaller than for the corresponding As-edge data and were consequently more difficult to fit. In fact, second-shell fits were only possible for $T_s \geqslant \sim 70$ °C; the deduced σ_2^2 values are included in figure 5. Although larger than the values deduced from As-edge EXAFS spectra, they appear to follow the same trend. The fitted values of r_2 were similar to those found from the As edges, lying between 3.95 and 3.99 Å. Ga-edge EXAFS from the GaAs crystal gave r_2 = 3.97 ± 0.03 Å and σ_2^2 = 0.014 ± 0.005 Å^2.

The fitted values of the interatomic distances and Debye–Waller factors allow us to calculate the bond angle θ and variation in bond angle $\Delta\theta$ from simple trigonometric considerations. Both As- and Ga-edge data give θ = 109° or 110° in all cases, confirming the tetrahedral nature of the structural network. $\Delta\theta_{Ga}$ deduced from As-edge EXAFS (i.e. the variation in bond angle around Ga atoms) is found to decrease from ±9° at substrate temperatures around room temperature to ±7° at $T_s \simeq 180$ °C. Ga-edge data indicate that $\Delta\theta_{As}$ (the bond-angle variation around As atoms) decreases from a value which is too large to measure at the lowest T_s values studied to ±9° at ∼ 180 °C. It should be pointed out that the deduced values of $\Delta\theta$ contain both structural and thermal contributions. Analysis of EXAFS measurements on c-GaAs, which is assumed to have only a thermal contribution to $\Delta\theta$, gave $\Delta\theta$ values of ±5° around both atom types. (Note that the second-shell peak in the Fourier transform disappears when $\Delta\theta$ is approximately double that in the crystal.

It has therefore been possible to show directly from EXAFS measurements that the bond-angle disorder around both atom types in the GaAs films decreases with increasing substrate temperature T_s. Over the range of T_s investigated, the variation in bond angle around Ga atoms is less than that around As atoms at a given

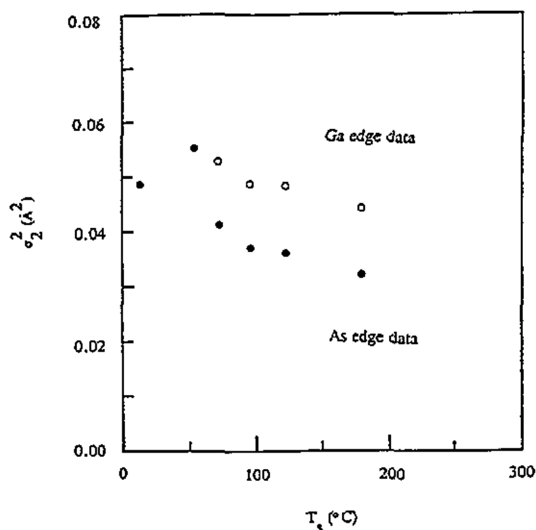

Figure 5. Second-shell Debye–Waller factors σ_2^2 as a function of T_s (substrate temperature during deposition) for both Ga- and As-edge data. The uncertainties in σ_2^2 are ±0.010 Å^2.

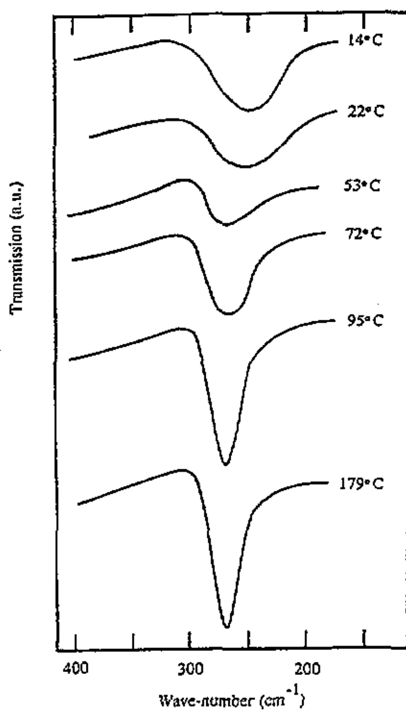

Figure 6. Infrared transmission spectra for sputtered GaAs samples. The substrate temperatures during deposition label the curves.

T_s. Tetrahedral structural units with Ga atoms at the centre are therefore less distorted than As-centred ones. Although TEM experiments revealed the presence of nanocrystallites for $T_s \geqslant \sim 70$ °C, the appearance of a second shell in the Fourier transforms of the EXAFS spectra reflects the increasing configurational order of the amorphous network rather than the appearance of the tiny nanocrystallites. σ_2^2 and $\Delta\theta$ for the sample prepared at ~180 °C are still appreciably larger than the corresponding values found for c-GaAs.

5.2. Core level spectra

The largest changes (with increasing T_s) in the XPS spectra of the GaAs films are expected in the valence band. However, the spectrometer resolution was relatively low compared to the energy separation of the observed features, and in this binding-energy range the signal-to-noise ratio was also low. We have therefore concentrated on information concerning the core levels, in particular the Ga and As 3d levels.

The Ga and As 3d spectra are similar for all sputtered and crystalline wafer samples; their positions and widths are detailed in table 1. As T_s is raised, both Ga and As levels show no changes in chemical shift (within experimental error) from those found for crystalline GaAs. This indicates that very few wrong bonds are present in all the samples, even those prepared at low T_s. There is, however, an indication from the energy differences of the Ga and As 3d levels (which are more accurate since the errors involved are mostly systematic) that there could be a small monotonic reduction in the density of wrong bonds with increase in T_s.

Table 1.

Sample	T_s = 53 °C	T_s = 72 °C	T_s = 179 °C	Crystalline wafer	Ga*	As*
Ga 3d	19.2	19.3	19.3	19.3	18.6	
FWHM	2.0	2.0	1.8	1.6		
Spin split			0.4	0.4		
Ga_2O_3	20.3	20.4	20.3	20.3		
As 3d	41.2	41.2	41.2	41.1		41.8
FWHM	1.9	1.9	1.7	1.6		
Spin split			0.4	0.4		
As 3d–Ga 3d	22.0	21.9	21.9	21.8		

Core level energies are given with respect to the Fermi level. All values are in eV and are ±0.1 eV. Values marked * are from [18].

The FWHM is governed not only by the instrumental linewidth but also by the spread in bond angle, i.e. the contribution from second-nearest neighbours. We find that the FWHM decreases monotonically with increasing T_s, implying a monotonic reduction in bond-angle disorder with increase in T_s, in line with the EXAFS data described in the previous section. The data suggests that even for the sample prepared at 179 °C, the bond-angle disorder is still appreciably greater than that in the crystalline material. Although indicated by the data, it is not possible to say with certainty that the spread in bond angle $\Delta\theta$ for Ga-centred tetrahedra is less than for As-centred tetrahedra, nor at what substrate temperature the main changes occur, because of the experimental errors involved. However, because of the reduction in FWHM, spin splittings can be measured for the samples deposited at higher T_s, and these are in line with those found for the crystalline material.

The findings described above are in overall agreement with the earlier work of Shevchik *et al* [19] who presented data for Ga 3d levels in amorphous and crystalline GaAs, deposited at 20 °C and 225 °C respectively, and also with the data of Senemaud *et al* [20] for an amorphous sample of GaAs which was then annealed to achieve crystallinity.

It would of course be of great interest to calculate *ab initio* the contribution to the chemical shifts expected due to the presence of wrong bonds and, similarly, the line broadening expected due to bond-angle disorder. Such calculations would, however, be very complicated and have not been attempted here. By decomposing the potentials seen by the core electrons into three parts involving that due to core charges on central atoms and nearest neighbours, bonding charge and a lattice contribution, it is possible to get at least a qualitative picture of the changes expected. In the elemental solid the terms will sum to zero, while in the stoichiometric crystal the cationic line shift is measured to be ~1 eV with respect to the Fermi level. Wrong bonds are expected to alter all three terms, the variation in bond length and sign of the charge causing the largest changes. Assuming a linear scaling, a shift of 0.1 ± 0.1 eV between the amorphous and crystalline samples (as measured) implies 10 ± 10% wrong bonds in the amorphous material. From our other data, it seems likely that the lower bound represents the more probable situation.

Bond-angle disorder is expected to change only the lattice term. Assuming a purely Coulombic interaction and a charge transfer of 0.25 electrons, a broadening of $E(\mathrm{eV}) = 14.4(q/r)$ may be expected, where q is the charge transfer in electrons and r is the distance from the outer core levels to the second-nearest neighbours in Ångströms. For the Ga 3d levels, this suggests broadenings of around 0.3 eV for a $\Delta\theta$ of ±11° (assumed value for T_s = 53 °C), 0.2 eV for a $\Delta\theta$ of ±9° (T_s = 179 °C) and 0.1 eV for ±5° (crystal). These values correspond within error to the changes in FWHM given in table 1.

5.3. Infrared data

Figure 6 shows infrared transmission spectra for some of the GaAs films over the wavenumber range 350–180 cm^{-1}. The strong absorption mode observed in each case is the Ga–As TO normal mode, which in c-GaAs is located at 268 cm^{-1}. No other features were observed over the entire range of wavenumbers available to us (4000–180 cm^{-1}) for any of the samples.

For the samples deposited at the two lowest temperatures, the TO mode is broad and centred at ~250 cm^{-1}. This is in good agreement with previous studies on a-GaAs which show a broadening and shift to lower wavenumber compared to the crystalline case [7, 21]. As can be seen from figure 6, the overall effect on the TO mode of raising T_s is a shift in position towards the crystalline value along with a sharpening and increase in intensity. For the sample prepared at ~50 °C (still completely amorphous according to TEM), the peak has shifted to ~270 cm^{-1} although it remains broad on the lower-wavenumber side. As T_s is further raised, the peaks continue to sharpen, becoming considerably more symmetric, although from figure 7, which shows the FWHM versus T_s, little further sharpening occurs above about 100 °C. Despite the appearance of the nanocrystallites at around 70 °C, the rapid shift to higher wavenumber and the sharpening of the Ga–As TO mode reflects the reduction in configurational (bond-angle) disorder of the amorphous network. For the samples prepared at the highest substrate temperatures, no additional modes (as would be expected in c-GaAs) were observed.

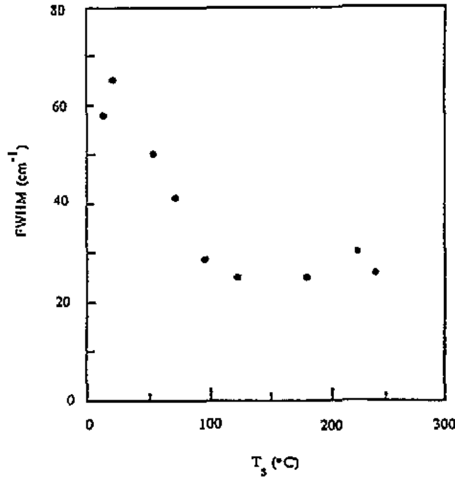

Figure 7. FWHM of Ga–As TO mode as a function of T_s.

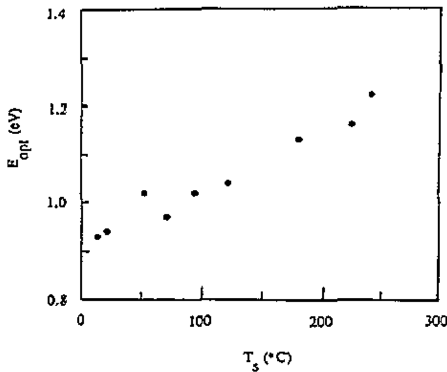

Figure 8. Optical (Tauc) gap E_{opt} as a function of T_s.

5.4. Optical gap and the absorption edge

The optical absorption coefficient α for the GaAs samples, measured by transmission and reflection methods as a function of photon energy $\hbar\omega$ in the visible and near-infrared region of the electromagnetic spectrum, was fitted to the Tauc relation

$$(\alpha\hbar\omega)^{1/2} = B(\hbar\omega - \mathrm{E}_{opt}) \tag{3}$$

in order to define an optical band gap E_{opt}. B is a constant. Figure 8 shows the deduced values of E_{opt} plotted as a function of T_s. For samples deposited at around room temperature, E_{opt} is approximately 0.95 eV which agrees reasonably with previous optical studies on a-GaAs [6, 7]. Bond-angle disorder in amorphous semiconductors normally give rise to a decrease in band gap; the gradual rise in E_{opt} with increasing T_s therefore appears to be consistent with a reduction in bond-angle variation. However, as O'Reilly and Robertson [22] have pointed out, the bandgap in amorphous III–V semiconductors may also be affected by defect states such as

dangling bonds; we shall discuss this point further in section 6. It should be noted that the optical gap for the samples prepared at highest T_s is still considerably less than the value in c-GaAs (~1.5 eV).

Our GaAs films were fairly thin, all film thicknesses lying between 0.09 and 0.16 μm. This tended to restrict the measurable range of α to rather high values. As mentioned in section 4.3. PDS experiments enable the measurement of lower absorption levels than are usually possible by conventional transmission and reflection techniques. Figure 9 shows examples of absorption curves (log α versus $\hbar\omega$) obtained by PDS, including the data obtained by transmission and reflection measurements, for the sputtered GaAs samples. The higher-energy part of the absorption curves ($\alpha \geqslant \sim 10^3$ cm^{-1}) shifts systematically to higher photon energy with increasing T_s, which is consistent with the observed increase in Tauc gap. However, at lower absorption levels, there is little or no such shift. The absorption edge therefore appears to broaden as T_s is raised; the Urbach edge parameter E_U, obtained by fitting the edge to the exponential relation

$$\alpha = \alpha_0 \exp(\hbar\omega / E_U) \tag{4}$$

increases gradually with rising T_s, from 50 meV for T_s = 14 °C to 74 meV for T_s = 223 °C, before increasing more rapidly to 120 meV for the sample prepared at 240 °C. At first sight, this broadening appears to be at odds with our other data as an increase in order normally gives rise to a sharpening of the absorption edge in amorphous semiconductors. However, as we shall discuss in the following section, this may not necessarily be so in amorphous III–V semiconductors.

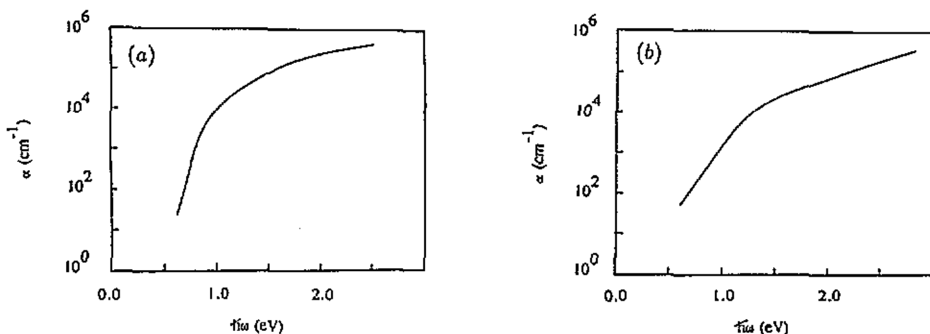

Figure 9. Absorption edge spectra for GaAs films sputtered at (*a*) 14 °C and (*b*) 240 °C.

All the values of E_U in our GaAs films, except for the sample deposited at 240 °C, are appreciably less than the figure of 110 meV measured by Theye *et al* [23] for flash-evaporated a-GaAs prepared at room temperature. These authors found that annealing such samples caused an essentially parallel shift of the absorption edge to higher energy with little change in E_U. Unfortunately, there have been few studies of the absorption edge in a-GaAs as a function of T_s or other deposition conditions. In sputtered material, Murri *et al* [24] found a decrease in E_U with increasing RF power (from ~260 meV at 100 W to ~140 meV at 400 W); a structural (TEM) study by the same authors [25] suggested that there was some increase in disorder as the power was raised. In the same study [25], TEM experiments revealed a change from an

amorphous to a nanocrystalline structure with increasing T_s over the range 20–155 °C; unfortunately, no E_U data are given for these samples.

6. Discussion

TEM experiments suggest that there is a relatively sharp transition in the structural nature of the sputtered GaAs films between (i) a purely amorphous network for substrate temperatures $T_s \leqslant \sim 50$ °C and (ii) an amorphous network in which there are tiny embedded nanocrystallites for $T_s \geqslant \sim 70$ °C. The size of the nanocrystallites increases gradually with rising T_s. Despite the appearance of such nanocrystallite inhomogeneities at relatively modest substrate temperatures, EXAFS and optical (including infrared) measurements all show that there is still much amorphous material in the structural network over the whole T_s range studied.

The structural picture for our sputtered GaAs films of nanocrystals embedded in an amorphous network (for $T_s \geqslant 70$ °C) is in good agreement with work by Zallen and co-workers [26–29] who, by means of Raman scattering experiments, investigated the structure of nanocrystalline GaAs layers produced by ion-bombarding crystalline wafers. The Raman spectra of such samples exhibited two-mode behaviour, with the crystalline LO (longitudinal optic) line superimposed on the Raman spectrum of a-GaAs (three broad overlapping bands, centred at approximately 70, 150 and 250 cm^{-1}). (Back-scattering geometry was adopted on (100)-oriented wafers so that only the $k = 0$ LO phonon, situated at 292 cm^{-1}, was Raman active in the crystal.) These results were taken as evidence that the ion-bombarded GaAs layers consisted of a fine-scale mix of a-GaAs and GaAs nanocrystals. From an asymmetric broadening and slight downward shift in wavenumber of the LO line with increasing ion bombardment, estimates were obtained for the size of the nanocrystals; values of between 50 and 100 Å were obtained [29] for various samples, in reasonable agreement with values measured by TEM for our sputtered samples.

Our EXAFS, XPS and infrared data confirm that raising the substrate temperature leads to a decrease in configurational disorder in the amorphous network of GaAs films. The EXAFS results not only demonstrate that most of this disorder relates to variation in bond angle (as opposed to variation in bond length) but also allow us to directly determine the bond-angle spread $\Delta\theta$. Our data show that $\Delta\theta$ around both atom types decreases as T_s is raised but that, at a given T_s, $\Delta\theta$ around Ga atoms is less than that around As atoms. With the assumption of a good degree of chemical ordering, this difference implies that tetrahedral units in the structure with Ga atoms at the centre become less distorted more easily than As-centred ones. A similar situation has recently been found in sputtered a-GaP films [9], the group V atom showing the greater spread in bond angle.

As was mentioned in section 5.4, bond-angle disorder normally causes some decrease in band gap in amorphous semiconductors. The increase in E_{opt} (figure 8) and the changes in the absorption curves at higher absorption levels (figure 9) with increasing T_s therefore appear to be consistent with improving order at higher T_s. However, calculations by O'Reilly and Robertson [22] on the local electronic structure of bulk and defect sites in amorphous III–V compounds (using the tight-binding recursion method) suggest that bond-angle disorder should result in hardly any decrease in band gap for these materials. If this is so, an alternative explanation is required to explain our absorption edge data.

The calculations by the above authors [22] suggest that dangling-bond states in a-GaAs are situated at or close to the band edges, with As dangling bonds near the valence band edge and Ga dangling bonds near the conduction band edge. This situation favours charge transfer from the higher Ga to the lower As dangling-bond level to produce a doubly occupied As level and an empty Ga level. Such transfer causes a downward shift of the As level and an upward shift of the Ga level tending to expel them from the gap. It also results in a relaxation of the bond angle at the dangling-bond sites from the tetrahedral bond angle towards the preferred angles of 97° in the case of As and 120° for Ga. In fact for all the amorphous III-V compounds investigated, O'Reilly and Robertson [22] calculated that relaxed anion dangling bonds occur at or below the valence band edge and relaxed cation dangling bonds occur at or above the conduction band edge. Furthermore, they suggested that such materials should contain a higher proportion of dangling bonds than a-Si. Although a fraction of about 3–4% broken bonds is expected in a-Si in order to reduce strain in the random tetrahedral network, most of these reconstruct to form weak bonds; in amorphous III–V compounds, which also have tetrahedral networks, a similar fraction of dangling bonds might be expected but it is suggested that these now relax rather than reconstruct. The picture described above for dangling bonds in a-GaAs may help to explain the absorption edge data for our GaAs films. As was seen in section 5.4, the optical gap and the region of the absorption curves corresponding to higher absorption levels shifted to higher energy with increasing T_s; this would then imply a decrease in dangling-bond density with increasing T_s, which is not perhaps surprising for an amorphous semiconductor.

The work of O'Reilly and Robertson [22] also predicts the energy levels of various wrong-bond defects in a-GaAs (and other related compounds). Isolated As–As bonds are calculated to give states just below the conduction band edge while isolated Ga–Ga bonds are predicted to give states just below the valence band edge. Clusters of wrong bonds and defect complexes are expected to produce states nearer midgap. If these calculations are correct, they suggest that the lower-energy part of our absorption curves (figure 9) may be associated with wrong-bond defects. The associated absorption levels are low which implies that we would be dealing with relatively small numbers of such defects (less than could be detected by EXAFS of infrared measurements at any rate). As we saw in section 5.4, the lower energy region of our absorption curves was much less affected by changing T_s than the higher-absorption part; this would indicate that the density of wrong-bond defects is much less affected by increasing T_s than the dangling bond density. If so, this could account for the observed broadening (increase in E_U) in our absorption edges as T_s is raised.

7. Conclusions

The structural (tetrahedral) network of sputtered GaAs films is purely amorphous for substrate temperatures T_s up to about 50 °C. For $T_s \geqslant \sim 70$ °C, the structure consists of nanocrystals embedded in an amorphous network. The average size of the nanocrystals increases as T_s is raised, reaching ~100 Å at ~180 °C.

Configurational disorder in the amorphous network of the GaAs films decreases with increasing T_s. Most of the disorder is associated with bond-angle (rather than bond-length) variation. For a given T_s, the spread in bond angle around Ga atoms is less than that around As atoms.

If the band gap in GaAs is little affected by bond-angle disorder (as some calculations suggest), the changes observed in the absorption edge spectra with increasing T_s are consistent with a reduction in dangling-bond density at higher T_s.

References

[1] Shevchik N J and Paul W 1974 *J. Non-Cryst. Solids* **13** 1
[2] Polk D E 1971 *J. Non-Cryst. Solids* **5** 365
[3] Connell G A N and Temkin R J 1974 *Phys. Rev.* B **9** 5323
[4] Dixmier J, Gheorghiu A and Theye M L 1984 *J. Phys. C: Solid State Phys.* **17** 2271
[5] Theye M L, Gheorghiu A and Launois H 1980 *J. Phys. C: Solid State Phys.* **13** 6569
[6] Gheorghiu A and Theye M L 1981 *Phil. Mag.* B **44** 285
[7] Baker S H, Manssor M I, Gurman S J, Bayliss S C and Davis E A 1992 *J. Non-Cryst. Solids* **144** 63
[8] Udron D, Flank A M, Gheorghiu A, Lagarde P and Theye M L 1989 *Phil. Mag. Lett.* **59** 9
[9] Elgun N, Gurman S J and Davis E A 1992 *J. Phys.: Condens. Matter* **4** 7759
[10] Paul W, Moustakas T D, Anderson D A and Freeman E 1977 *Proc. 7th Int. Conf. on Amorphous and Liquid Semiconductors (Edinburgh, 1977)*
[11] Hargreaves M, Thompson M J and Turner D 1980 *J. Non-Cryst. Solids* **35 & 36** 403
[12] Matsumoto N and Kumabe K 1980 *Japan. J. Appl. Phys.* **19** 1583
[13] Morrell C, Campell J C, Diakun G P, Dobson B R, Greaves G N and Hasnain S S *EXAFS Users' Manual* (Daresbury: SERC)
[14] Gurman S J, Binsted N and Ross I 1984 *J. Phys. C: Solid State Phys.* **17** 143
[15] Bayliss S C, Baker S H and Gurman S J in preparation
[16] Bayliss S C and Gurman S J 1991 *J. Non-Cryst. Solids* **127** 174
[17] Singh A, Bayliss S C, Gurman S J and Davis E A 1992 *J. Non-Cryst. Solids* **142** 113
[18] Anthony M T 1983 *Practical Surface Analysis by Auger and XPS* (New York: Wiley) ed D Briggs and M P Seah pp 498–9
[19] Shevchik N J, Tejeda J and Cardona M 1974 *Phys. Rev.* B **15** 2627
[20] Senemaud C, Belin E, Gheorghiu A and Theye M L 1985 *Solid State Commun.* **55** 947
[21] Wang Z P, Ley L and Cardona M 1982 *Phys. Rev.* B **26** 3249
[22] O'Reilly E P and Robertson J 1986 *Phys. Rev.* B **34** 8684
[23] Theye M L, Gheorghiu A, Driss-Khodja K and Boccara C 1985 *J. Non-Cryst. Solids* **77 & 78** 1293
[24] Murri R, Schiavulli L, Pinto N and Ligonzo T 1992 *J. Non-Cryst. Solids* **139** 60
[25] Murri R, Gozzo F, Pinto N, Schiavulli L, De Blasi C and Manno D 1992 *J. Non-Cryst. Solids* **127** 12
[26] Holtz M, Zallen R and Brafman O 1988 *Phys. Rev.* B **37** 2737
[27] Holtz M, Zallen R, Brafman O and Matteson S 1988 *Phys. Rev.* B **37** 4609
[28] Zallen R, Holtz M, Geissberger A E, Sadler R A, Paul W and Theye M L 1989 *J. Non-Cryst. Solids* **114** 795
[29] Zallen R 1992 *J. Non-Cryst. Solids* **141** 227